AIP | Journal of Applied Physics

Neutralization efficiency estimation in a neutral beam source based on inductively coupled plasma

O. V. Vozniy and G. Y. Yeom

Citation: J. Appl. Phys. **105**, 013308 (2009); doi: 10.1063/1.2987475
View online: http://dx.doi.org/10.1063/1.2987475
View Table of Contents: http://jap.aip.org/resource/1/JAPIAU/v105/i1
Published by the American Institute of Physics.

Neutralization efficiency estimation in a neutral beam source based on inductively coupled plasma

O. V. Vozniy[1,2] and G. Y. Yeom[1,a)]
[1]*Sungkyunkwan Advanced Institute of Nano Technology (SAINT), Sungkyunkwan University, Jangan-Gu Chunchun-Dong 300, Suwon 440-746, Republic of Korea*
[2]*Kharkiv Scientific Center of Physics and Technologies, 6 Svobody sq, Kharkiv 61077, Ukraine*

(Received 14 April 2008; accepted 8 August 2008; published online 9 January 2009)

This study examined the optimal conditions of neutral beam generation to maintain a high degree of neutralization and focusing during beam energy variation for a neutral beam source based on inductively coupled plasma with a three-grid ion beam acceleration system. The neutral beam energy distribution was estimated by measuring the energy profiles of ions that "survived" the neutralization after reflection. The energy measurements of the primary and reflected ions showed narrow distribution functions, each with only one peak. At higher beam energies, both the ratio of the ion energy loss to the primary energy and the degree of energy divergence decreased, confirming the precise alignment of the neutral beam. The neutralization efficiency of the neutral beam source with a three-grid acceleration system was found to be affected mainly by the beam angle divergence rather than by the particle translation energy. © *2009 American Institute of Physics*.
[DOI: 10.1063/1.2987475]

I. INTRODUCTION

The recent development of neutral beam technology[1–5] has increased the effectiveness of this type of surface treatment for the etching and deposition of nonconducting or low-conductivity materials that are free of the undesirable consequences due to the presence of charge at the sample surface. Damage, such as trenches caused by beam deviation in an electric field of the charged surface, and electronic structure modification due to ion implantation can cause irreversible changes to the sample properties.[6–10] Therefore, a method of physical and chemical etching using a neutral beam is a promising alternative to ion-beam treatment. The application of neutral beam technology has decreased both the appearance of structural defects and the portion of particles reacting with the atoms of the working and residual gases in the beam transportation region because neutral radicals are less chemically active than ions.

Several attempts have been made to generate a neutral beam of sufficiently high flux and narrow energy distribution. Charge exchange of the primary ion beam occurs either with the atoms of the residual gas during beam transportation in the region of increased pressure[11–13] or with the surface atoms during ion scattering by the grounded conducting materials.[14,15] The energy distribution function of neutral particles generated by sources of the first type is quite broad and often has several peaks, while the lack of strict beam directionality prevents its application to nanotechnology. Sources of the second type are more promising because in this case the parameters of the primary ion beam and the neutral beam are similar. The resulting flux of neutral atoms or radicals here depends on the probability of electron tunneling due to Auger or resonant processes from the reflecting surface to the excited or ground states of the fast ion.

To increase the range of industrial applications for these systems, it is essential to solve a number of problems, including the direct measurement of the main neutral beam parameters, such as the molecular composition, energy, and angular distribution. The implementation of additional ionization of the atomic flux for these purposes is difficult due to the small ionization cross section. The ionization efficiency is proportional to $E_I^{-1/2}$, where E_I is the ion energy, so that the apparatus for detection is only sensitive to low-energy particles. Some studies reported the flux of ionized neutrals to be as small as 100 times lower than the background ion current originating from the plasma.[16] It is impossible to remove this residual current, even after applying a high voltage to a repelling grid installed between the neutral beam source and the analyzer. This grid not only decreases the particle flux due to its limited transparency, but also allows ionizing ultraviolet radiation to pass from the plasma. Eventually, the two ion groups overlap, making their separation difficult due to the large energy and angle dispersion of the resulting flux.

The problem of neutral beam analysis can be simplified if it is considered that a major part of the energy loss occurring during ion collision with the surface is consumed not by the neutralization process but by the elastic collisions of the particle with the surface atoms, as previously reported.[17–19] Nonionizing diagnostics allows the measurement of only that part of the energy that is transferred to the surface as a result of elastic collisions, while methods employing additional ionization can provide the magnitude of the total energy loss but with low accuracy.

An analysis of the energy spectra of the electrons emitted from the surface during Auger neutralization (AN) proves that the magnitude of energy loss during the neutralization process is significantly lower than that due to elastic collisions[20] and does not depend on the initial particle en-

a)Electronic mail: gyyeom@skku.edu.

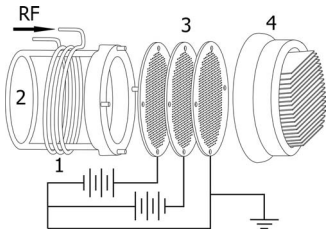

FIG. 1. Experimental setup for the low-angle forward-reflected neutral beam source. 1 rf antenna, 2 quartz chamber, 3 electrostatic electrodes, 4 reflector.

ergy. Therefore, the energy and angular characteristics of the neutral beam and the beam of ions which survived neutralization are interrelated.

In this paper, the parameters of the reflected beam such as energy, angular distribution, and neutralization efficiency are estimated and correlated. The finding of a correlation function between the energy of the primary ion beam and the energy of the reflected particles might allow a comparison of the parameters of both fluxes, thereby allowing this method to be used as an effective instrument for examining the performance of neutral beam sources.

II. EXPERIMENT

Figure 1 shows a schematic diagram of the neutral beam source. High-density plasma was generated inside quartz chamber 2 after 13.56 MHz radio frequency power (ENI RF 20S generator) was delivered to a three-turn coil through a π-type matching network.

Focusing and formation of the positive ion beam was made with the system of grid electrodes 3. The first grid electrode contacting the plasma was designated to increase the plasma potential to the required level.[21] The second negatively charged electrode enabled control of the degree of beam focusing due to the suppression of plasma molding near the apertures of the first grid. The third grounded grid electrode was designed to eliminate ions leaving the source under high angles relative to the axis of beam transportation and to screen the field of the second electrode. In all measurements, Ar was used as the working gas with a constant flow rate of 7 SCCM (SCCM denotes standard cubic centimeter per minute at STP). The pressure in the beam transportation region did not exceed 2×10^{-4} Torr. The rf generator output power was fixed at 200 W.

The primary ion beam was neutralized during the glancing scattering from reflector 4, which represented a set of polished metal plates parallel to each other. The angle between the plates and the main axis of the source could be varied from 3° to 15° and a reflection angle of 5° was chosen in these experiments because it effectively neutralized the ion beam and prevented the ions that did not collide with the surface from leaving the source and reaching the energy analyzer.

The ion current density of the primary and reflected beams was measured using a planar Langmuir probe placed 1 cm from the source. Radio frequency noise from the probe was eliminated using an adapted *LC* filter. The ion energy distribution function (IEDF) was measured using a quadrupole mass spectrometer (Hiden Analytical Inc. EQP-1000) with an integrated 45° sector field energy analyzer, which determined the energy profiles of positively charged ions with a resolution of 0.1 eV in the static regime and in the regime of variation of the beam parameters in time.

III. RESULTS AND DISCUSSION

In order to study the neutralization process in a neutral beam source based on inductively coupled plasma (ICP), it is convenient to distinguish two interaction mechanisms of the particle with the surface atoms: collisions with the electrons (internal energy transfer), when a fast ion causes excitation or ionization of the lattice atom, and collisions with the nucleus (kinetic energy transfer). Since the electron density in the solid is high, there are many collisions of the first type, which are often believed to be steady. In the case of kinetic energy transfer, which is significantly less frequent, only an interaction between the screened nucleus of the primary ion and the surface atoms is considered. Therefore, they can be treated as separate events. The behavior of the high and middle energy ions during the scattering was described sufficiently well with the Rutherford screened Coulomb potentials. However, at low energies, the characterization of the interaction mechanism becomes rather complicated.

A. Kinetic energy transfer

Despite the variety of processes occurring during ion neutralization, the energy loss by the particle due to electron capture does not exceed several eV and depends only implicitly on the magnitude of the translational energy because it is determined only by the atom ionization energy and the metal conduction band structure.[22] The largest part of the energy loss is believed to be caused by elastic collisions, i.e., by a process where the energy is not spent for electron state excitation.

The theory of binary collisions provides the approximate magnitude of energy loss when it is assumed that the surface atoms, which are not directly involved in the collision process, do not significantly alter the trajectory of the reflected particle.[23] The solution of the energy and momentum conservation equations gives the magnitude of the energy loss of the ion during its reflection from the surface[24] as follows:

$$\Delta E_N^{\mathrm{sc}} = E_I\left\{1-\left[\frac{\mu}{1+\mu}(\cos\theta_0+\sqrt{1/\mu^2-\sin^2\theta_0})\right]^4\right\}, \quad (1)$$

where $\mu=m_M/m_{\mathrm{Ar}}$, m_M and m_{Ar} are the surface and projectile atomic masses, respectively. E_I and E_N^{sc} are the particle energy before and after collision, respectively, and θ_0 is the angle of incidence.

It is noteworthy that the magnitude of the total energy loss $\Delta E_t=\Delta E^n+\Delta E_N^{\mathrm{sc}}$, where ΔE^n is the energy loss due to electron energy transfer, cannot be established reliably, since ΔE^n can be studied only implicitly by analyzing the energy distribution function of the electrons emitted from the metal surface.[25] There is also the possibility of additional ionization of the neutral beam, which will enable further energy analysis. However, it should be noted that during this procedure, the projectile particle energy change in this case is comparable to ΔE^n. At the same time, ΔE^{sc} can be measured

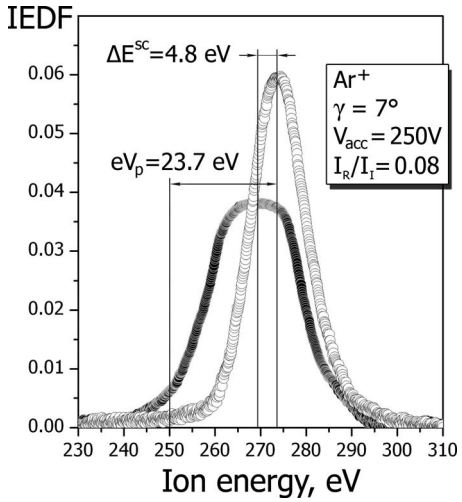

FIG. 2. Normalized IEDFs for the primary (white symbols) and reflected (dark symbols) ion beams.

directly during the study of the ions that "survived" neutralization during the reflection from the surface.

The current of reflected ions is significantly lower than the primary ion current, and its distribution function shows wide scatter. Since the intensity of the detected signal depends on the beam energy, normalization of the IEDF is required to determine energy loss during elastic collisions for specific beam energy. Figure 2 shows the normalized energy distribution functions for both currents that satisfy the following condition:

$$\int_0^\infty f_{I,R}(E)dE = 1. \tag{2}$$

Normalization was performed after the IEDF measurements in addition mode, which allowed averaging the current of the "surviving" ions. The data obtained from the primary beam measurements did not require such a procedure. The maximum of the energy distribution function for the primary beam is shifted relatively to the preset value eV_{acc} by the magnitude eV_p, where V_p is the plasma potential. At the same time, the maximum of the energy distribution of the reflected ion beam is determined by the shift in $eV_p - \Delta E^{\mathrm{sc}}$.

Reflection of the particle from the metal surface not only shifts the energy distribution, but also increases the beam energy spread, which has an adverse effect on the etching selectivity and anisotropy. Therefore, the conditions at which energy deviation of the beam particles from the preset value has its minimum should be found. The energy spread divergence η was calculated by the following formula:

$$\eta = \frac{\int_0^\infty |f_R(E) - f_I(E + \Delta E^{\mathrm{sc}})|dE}{\int_0^\infty f_R(E)dE} = \frac{\int_0^\infty |f_R(E - \Delta E^{\mathrm{sc}}) - f_I(E)|dE}{\int_0^\infty f_I(E)dE}. \tag{3}$$

Figure 3 shows its dependence against the beam energy, as well as the difference in the mean energies of the primary and the reflected beams,

$$\langle E_I \rangle - \langle E_R \rangle = \frac{\int_0^\infty f_I(E)EdE}{\int_0^\infty f_I(E)dE} - \frac{\int_0^\infty f_R(E)EdE}{\int_0^\infty f_R(E)dE}. \tag{4}$$

The mean ion energy difference and the energy spread divergence have a similar dependence on the beam energy. The energy spread of the primary beam remains almost unchanged due to the constancy of the potential drop near the acceleration electrode. At the same time, the energy spread of the reflected beam decreases despite the increasing energy loss in elastic collisions. This is a result of the increase in beam focusing at higher energies because the energy can only be increased by increasing the focusing potential,[26] which suppresses plasma molding near the apertures of the first electrode. As a result, more ions are reflected from the surface at the optimal angle.

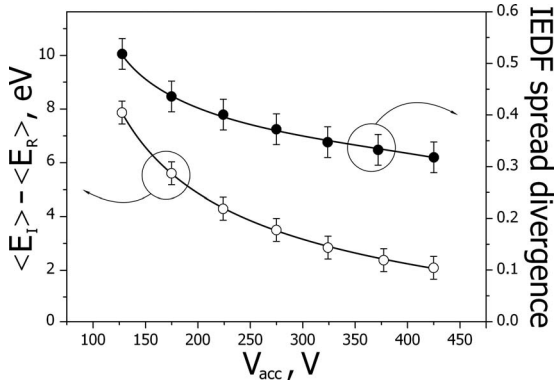

FIG. 3. Mean energy difference of the primary and reflected ion beams, and the energy distribution spread divergence as a function of the beam energy.

B. Electron energy transfer

Only nonradiating electron transitions, such as AN and resonant neutralization (RN), are possible during the scattering because ions spend a short period of time near the surface ($<10^{-2}$ s). Figure 4 shows a schematic diagram of both processes.

Only one electron is involved in the RN process. When the projectiles approach the surface with energy levels shifted upwards by a dielectric response ($\Delta E_i, \Delta E_{\mathrm{ex}}$), an electron transition occurs (it is denoted as RN) from the filled energy level of the metal to an excited or ground state of the ion, in which energy is lower than the Fermi level. This type of neutralization is dominant only when the condition $W < E_I < W + E_F$ is fulfilled, where E_I is the ion initial energy. At the same time, AN always occurs when $W < E_I$.

During AN, electron capture from the n-level of the surface causes energy transfer to the m-level electron ($E_{\mathrm{en}} > E_{\mathrm{em}}$). This is followed by the m-electron emission, which is always observed near the reflecting surface. This process can be written as

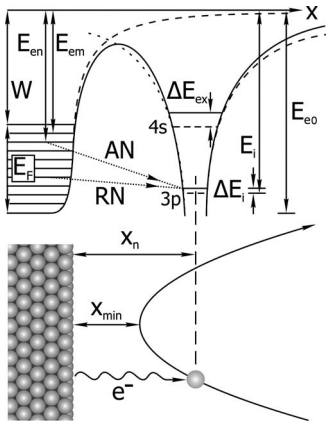

FIG. 4. Schematic diagram of AN, and RN and de-excitation during Ar+ interaction with the reflector. The dashed lines at the top represent the undisturbed surface potential and atom energy levels.

$$\mathrm{Ar}^+ + e_n^- + e_m^- = \mathrm{Ar}^0 + e_0^-. \tag{5}$$

From energy conservation law, the energy before the neutralization can be expressed as follows:

$$E_I + E_i + E_{\mathrm{IM}} - (E_{e0} - E_{\mathrm{en}}) - (E_{e0} - E_{\mathrm{em}}). \tag{6}$$

This should be equal to the energy of the system after electron capture by the ion

$$E_N + E_{\mathrm{NM}} + (E_e - E_{eo}), \tag{7}$$

where E_{e0} is the energy of the lowest Fermi level, E_e is the energy of the free electron, E_{IM} and E_{NM} are the particle-metal Coulomb interaction energies at the distance x_n for the ion and the neutral atom, respectively, and E_i is the ionization energy. Therefore, the particle should suffer an energy loss that is equal to

$$\Delta E^n = E_N - E_I = +E_i'(x_n) + 2\varepsilon - E_e - E_{e0}, \tag{8}$$

where $2\varepsilon = E_{\mathrm{en}} + E_{\mathrm{em}}$ and $E_i'(x_n) = E_i + E_{\mathrm{IM}} - E_{\mathrm{NM}}$, which is the effective ionization energy of a given atom at the distance x_n.

When the ion captures an electron in front of the metal surface, it gets an energy corresponding to the image potential $\Delta E_g = E_{N\perp} - E_{I\perp}$. Since $E_{I\perp} \sim v^2$, $E_{I\perp} = E_I \sin^2\theta \approx E_I \cdot \theta^2$. Thus when the image charge interaction energy is approximated by the simple classical limit $-1/4x$, the reflection angle θ can be written as a function of x_n,

$$\theta^2 - \theta_0^2 = -\frac{1}{4E_I x_n}. \tag{9}$$

Auger de-excitation also can be an alternative neutralization process when $W < E_I$. It occurs when the capture of the Auger electron to the excited ion level is followed by system relaxation to a steady state. Under the conditions realized in the neutral beam source, when the ion is neutralized at the metal plate, the probability of Auger de-excitation and RN is significantly lower than the probability of Auger tunneling to the ground state of the atom.

C. Angular distribution of scattered particles

In 1954, Hagstrum[20] defined transition rate $\Gamma(x)$, such that $\Gamma(x)dx/v(x)$ is the probability that a particle with velocity $v(x)$ will undergo neutralization at the distance interval dx from the surface. Then the probability that the particle reaches x without neutralization is

$$P^+(x, v) = \exp\left[-\int_x^\infty \frac{\Gamma(x)}{v(x)}dx\right], \tag{10}$$

which is a particular solution of the following equation:

$$\frac{dP^+(t)}{dt} = -\Gamma(x)P^+(t). \tag{11}$$

Relation (11) defines the neutral fraction N_a in reflected beam, so that

$$\frac{dN_a}{dt} = \Gamma[x(t)](1 - N_a). \tag{12}$$

Later the magnitude of the characteristic velocity $v_c = \int_0^\infty \Gamma(x)dx$ was introduced[27] to indicate the exponential dependence of N_a against particle speed. Its physical meaning defines the particle energy $E_c = mv_c^2/2$ when $x_n \to x_{\min}$, where x_n is the most probable distance at which AN occurs. Thus, the probability of escaping neutralization for the particle is $P_{\mathrm{in}}^+ \cdot P_{\mathrm{out}}^+$, where P_{in}^+ and P_{out}^+ are the corresponding probabilities on inward and outward trajectories

$$P_{\mathrm{in}}^+ \cdot P_{\mathrm{out}}^+ = \exp\left\{-\sqrt{\frac{E_c}{E_{I\perp}}} - \sqrt{\frac{E_c}{E_{N\perp}}}\right\}. \tag{13}$$

Differentiation of $P_{\mathrm{in}}^+ \cdot P_{\mathrm{out}}^+$ with respect to θ gives the following equation for angular distribution $F[\theta(x)]$,

$$\frac{\partial F[\theta(x)]}{\partial \theta} = \frac{\partial P_{\mathrm{in}}^+(\theta)}{\partial \theta} P_{\mathrm{out}}^+(\theta) + P_{\mathrm{in}}^+(\theta)\frac{\partial P_{\mathrm{out}}^+(\theta)}{\partial \theta}. \tag{14}$$

Using Eq. (10), it is easy to show that the density of this distribution $f[\theta(x)] = \partial F[\theta(x)]/\partial\theta$ is equal to

$$f[\theta(x)] = \sqrt{\frac{2m}{E_I(x)}}\Gamma(x)\exp(\xi|_{x=\infty})\cosh(\xi)\left|\frac{\partial x}{\partial \theta(x)}\right|, \tag{15}$$

where

$$\xi(x) = \int_{x_{\min}}^x \Gamma(x)\sqrt{\frac{m}{2E_I(x)}}dx. \tag{16}$$

Equation (15) is a general solution of Eq. (14), which takes into account the dependence of the ion energy against distance between the surface and the projectile ion during the whole interaction process.

Figure 5 shows the ion angular distribution function for the 300 and 400 eV beams, as well as the modeling result of $f(\theta)$ by the solid lines, where the function $\Gamma(x)$ represents exponential decay and $E_I(x) = \mathrm{const}$.

The measure of primary beam defocusing in neutral beam source, i.e., its angular divergence, is the loss current on the second grid electrode. These losses can be measured when a small negative bias is applied to the grid to exclude the electron current from the measured signal. Figure 6 shows the loss current dependence as a function of the focusing potential. The acceleration voltage was varied from 0 to 800 V. At the initial part of the curve, where an abrupt increase in loss current was observed, focusing by using the

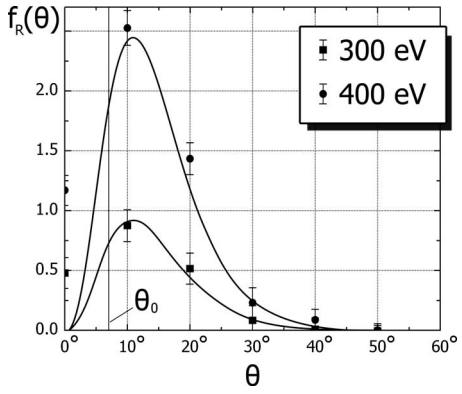

FIG. 5. Angular distribution of the neutral beam obtained from the beam etching rate measurements and the corresponding results of the angular distribution modeling for 300 and 400 eV beams.

three-grid system was impossible due to the high value of plasma potential, which might exceed the accelerating voltage at low beam energies.[28] Beam formation from the random flux occurred only when the acceleration voltage was several times higher than the plasma potential. A minimum of loss current was observed when the acceleration voltage approached 800 V, which corresponded to the highest degree of the primary beam alignment.

Figure 7 shows the dependences of the primary and reflected ion currents against the focusing potential. $j_R(E)$ was multiplied by the coefficient $1/(1-\gamma_0)$ for clarity, where γ_0 is the beam neutralization efficiency in the absence of accelerating voltage, which corresponds to a focusing potential of V_f=200 V between the first and second electrodes. As shown in Fig. 7, the magnitude of the reflected ion beam current is determined by the degree of beam focusing, since the neutralization efficiency can be improved by increasing the number of ions reflected from the surface under smaller angles. It is convenient to use the following magnitude:

$$\Delta = j_I - \frac{j_R}{1-\gamma_0}, \tag{17}$$

which can be measured easily to determine the dependence of the neutralization efficiency against the focusing potential, so that

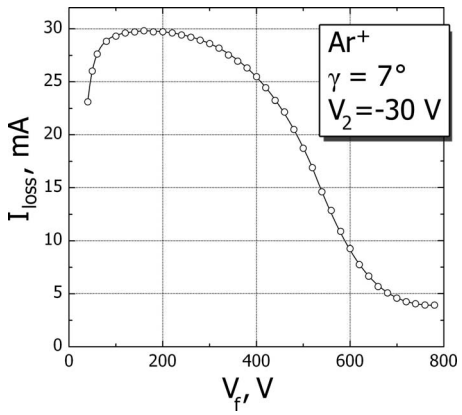

FIG. 6. Loss current at the second electrode as a function of the focusing potential.

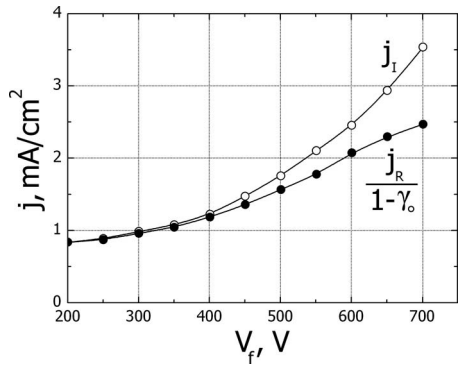

FIG. 7. Primary and reflected ion beam current growth as a function of the focusing potential.

$$\gamma = \gamma_0 + \frac{\Delta}{j_I}(1-\gamma_0). \tag{18}$$

D. Neutralization efficiency measurements

The specific feature of the neutralization efficiency measurements against the beam energy is conditioned by the increasing magnitude of the output current with increasing acceleration voltage due to the reduced ion loss on the second electrode. Therefore, in order to determine the portion of neutralized ions, there is a need to normalize the current of the reflected particles to the magnitude of the primary ion current. This can be performed by current measurements of the primary and reflected beams while keeping constant either the focusing potential $V_f=V_1-V_2$ or the second grid voltage V_2. Figures 8 and 9 show these dependences when V_f=400 V and V_2=−200 V. In the first case, the magnitude of the potential drop near the surface of the first electrode was almost constant, so that the ion current loss on the second electrode decreased more slowly with increasing beam energy. As is shown in Fig. 9, when V_2=const and the energy increased, plasma surface smoothing near the electrode holes significantly increased the primary and reflected currents.

Figure 10 shows the corresponding neutralization efficiencies for both measuring procedures. For all energy intervals, the current of the reflected ions was not linearly proportional to the primary ion current. However, the normalization of the current when V_2 is constant appeared to

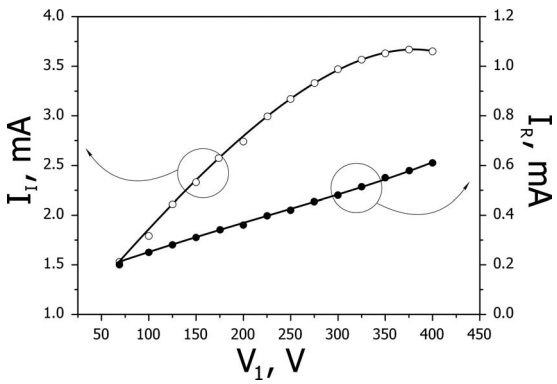

FIG. 8. Primary and reflected ion beam currents as a function of the acceleration potential at $V_f=V_1-V_2$=const.

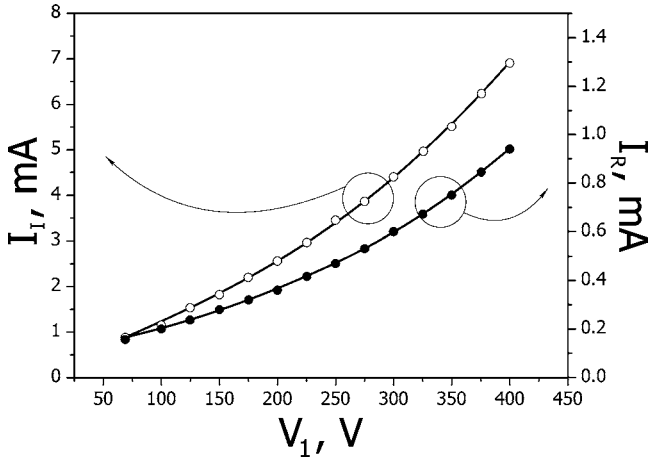

FIG. 9. Primary and reflected ion beam currents as a function of the acceleration potential at V_2=const.

be more reliable because ion current saturation on the second electrode was not observed using this method. The peak at low energy for both dependences was associated with the plasma potential drop near the first electrode. The number of surviving ions decreased with increasing energy due to the decrease in $x_{\min}$ because the probability of AN is exponentially dependent on it.[29] The neutralization efficiency remains constant when the perpendicular component of the ion translational energy $E_{\perp} > 25$ eV at V_2=const. This confirms the dominance of AN, which does not directly depend on the ion energy. The growth of the reflected ion current at V_f=const at such energies can be explained by the large angular spread of the primary ion beam, which decreases the probability of AN.

Figure 11 shows the dependence of the neutralization efficiency on the beam energy and focusing potential between the first and second electrodes. When $E_I < 200$ eV, the neutralization efficiency showed a stronger dependence on the particle translation energy than on the focusing potential, but this trend was reversed at higher energy when the second grid potential not only increased the neutralization probability but also improved the beam directionality.

IV. CONCLUSIONS

This study has examined the process of ion beam neutralization in an ICP-based neutral beam source. Ions were produced in discharge volume and accelerated by a system of grid electrodes. The last stage of neutral beam formation was the scattering of the ion beam by a set of conductive plates under grazing angles. Such sources may be useful for preventing charging damage in the fabrication of the next generation of microelectronic devices.

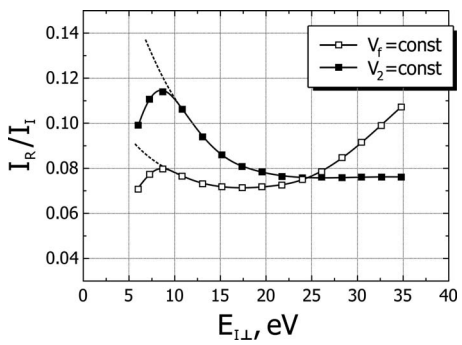

FIG. 10. Ratio of the reflected ion current and the primary ion current for two normalization methods. The dashed lines represent these dependences in the absence of the plasma potential influence on the ion current.

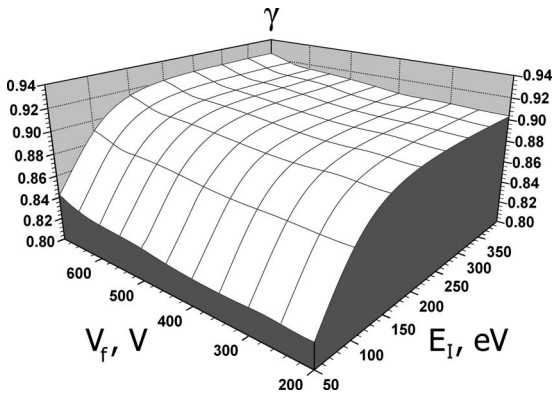

FIG. 11. Neutralization efficiency of the Ar beam as a function of the beam energy and focusing potential.

Although AN is the main mechanism of charge exchange between the surface and the ion beam, it was found that the largest part of the energy loss was caused by elastic collisions rather than by the interaction of electron shells of the projectiles and the surface atoms. Ion energy profiles of the direct and reflected beams were obtained. The magnitude of energy loss due to elastic collisions was estimated, as well as the evolution of ion energy distribution for different parameters of ion extraction.

The angular distribution of reflected particles was calculated for the case when the transition rate is exponentially dependent on the distance between the ions and the surface. The modeling results were compared with the experimental data and the small mismatch was explained by the fact that the primary ion beam was not strictly directional. To account for the initial divergence of the beam, the dependence of the loss current against the focusing potential was measured. The loss current was minimized at high voltages between the first and second electrodes, which allowed the source to be operated at optimal conditions.

Two methods of neutralization efficiency measurement were proposed. The first maintained focusing potential and loss current constant, while in the second the second grid potential was unaltered. The corresponding dependences of the neutralization efficiencies against beam energy and focusing potentials were obtained for both methods.

ACKNOWLEDGMENTS

This study was supported by the National Program for Tera-level Nanodevices of the Korean Ministry of Science and Technology as one of the 21st Century Frontier Programs.

[1] S. Noda, H. Nishimori, T. Iida, T. Arikado, K. Ichiki, T. Ozaki, and S. Samukawa, J. Vac. Sci. Technol. A **22**, 1506 (2004).
[2] H. Ohtake, N. Inoue, T. Ozaki, and S. Samukawa, J. Vac. Sci. Technol. B **23**, 210 (2005).

[3]S. Samukawa, K. Sakamoto, and K. Ichiki, J. Vac. Sci. Technol. A **20**, 1566 (2002).
[4]S. Panda, D. J. Economou, and L. Chen, J. Vac. Sci. Technol. A **19**, 398 (2001).
[5]M. J. Chung, D. H. Lee, and G. Y. Yeom, Thin Solid Films **420–421**, 579 (2002).
[6]T. Kinoshita, M. Hane, and J. P. McVittee, J. Vac. Sci. Technol. B **14**, 560 (1996).
[7]H. Hashimoto, Jpn. J. Appl. Phys., Part 1 **33**, 6013 (1994).
[8]S. G. Ingram, J. Appl. Phys. **68**, 500 (1990).
[9]G. S. Hwang and K. P. Giapis, J. Appl. Phys. **82**, 566 (1997).
[10]J. C. Arnold and H. H. Sawin, J. Appl. Phys. **70**, 5314 (1991).
[11]T. Yunogami, K. Yogokawa, and T. Mizutani, J. Vac. Sci. Technol. A **13**, 952 (1995).
[12]T. Mizutani and T. Yunogami, Jpn. J. Appl. Phys., Part 1 **29**, 2220 (1990).
[13]H. Kuwano and F. Shimokawa, J. Vac. Sci. Technol. B **6**, 1565 (1988).
[14]Y. Jin, T. Tsuchizawa, and S. Matsuo, Jpn. J. Appl. Phys., Part 2 **34**, L465 (1995).
[15]X. Tang, Q. Wang, and D. M. Manos, J. Vac. Sci. Technol. B **18**, 1262 (2000).
[16]A. Ranjan, V. M. Donnelly, and D. J. Economou, J. Vac. Sci. Technol. A **24**, 1839 (2006).
[17]H. Yamamoto, Y. Baba, and T. A. Sasaki, Appl. Surf. Sci. **100–101**, 333 (1996).
[18]S. Noda, H. Nishimori, T. Ida, T. Arikado, K. Ichiki, T. Ozaki, and S. Samukawa, J. Vac. Sci. Technol. A **22**, 1506 (2004).
[19]F. Shimokawa and H. Kuwano, J. Vac. Sci. Technol. **72**, 13 (1992).
[20]H. D. Hagstrum, Phys. Rev. **96**, 336 (1954).
[21]R. J. Taylor, K. R. MacKenzie, and H. Ikezi, Rev. Sci. Instrum. **43**, 1675 (1972).
[22]A. Sindona, R. A. Baragiola, S. Maletta, G. Falcone, A. Oliva, and P. Riccardi, Nucl. Instrum. Methods Phys. Res. B **230**, 298 (2005).
[23]H. Niehus, W. Heiland, and E. Taglauer, Surf. Sci. Rep. **17**, 213 (1993).
[24]A. Helmer and D. B. Graves, J. Vac. Sci. Technol. A **16**, 3502 (1998).
[25]R. A. Baragiola, *Low Energy Ion–Surface Interaction* (Wiley, New York, 1994), p. 187.
[26]I. G. Brown, *The Physics and Technology of Ion Sources*, 2nd ed. (Wiley, New York, 2004).
[27]M. Draxler, R. Gruber, H. H. Brongersma, and P. Bauer, Phys. Rev. Lett. **89**, 263201 (2002).
[28]O. V. Vozniy, B. J. Park, K. S. Min, and G. Y. Yeom, J. Korean Phys. Soc. **50**, 1271 (2007).
[29]M. A. Cazalilla, N. Lorente, R. Díez Muino, J.-P. Gauyacq, D. Teillet-Billy, and P. M. Echenique, Phys. Rev. B **58**, 13991 (1998).